Progress In Electromagnetics Research B, Vol. 50, 19–36, 2013

ELECTROMAGNETIC IMAGING OF DIELECTRIC CYLINDERS BY DIFFERENTIAL EVOLUTION AND SINGLE INTEGRAL EQUATION

Krzysztof A. Michalski*

Department of Electrical and Computer Engineering, Texas A&M University, College Station, TX 77843-3128, USA

Abstract—A technique is described for the electromagnetic reconstruction of the location, shape, dielectric constant, and conductivity of buried homogeneous cylinders of elliptic cross-section. The inversion procedure is based on the Differential Evolution algorithm and the forward problem is solved using the single boundary integral method. Simulation results are presented which demonstrate that this hybrid approach can offer a conceptually simple yet efficient and reasonably robust method for the imaging of buried objects and voids.

1. INTRODUCTION

The electromagnetic (EM) imaging of unknown objects located in inaccessible domains is a challenging problem with applications in many areas, such as remote sensing, noninvasive testing, and landmine localization — just to name a few [1–3]. Recently, genetic algorithms (GAs) [4, 5], which belong to a class of stochastic search techniques, have found extensive applications in the EM reconstruction of impenetrable and dielectric cylinders [6–10]. The advantage of GAs is that they usually yield the global optimum, while being simple to apply, because the derivatives of the objective function are not required. On the other hand, GAs tend to be computationally expensive, which prompted the development of many variants of the basic GA. One of the recent significant developments in this area was the invention of the Differential Evolution (DE) algorithm [11, 12], which has been shown to outperform other known global optimization methods on a number of synthetic problems [13, 14]. Since its introduction, DE is rapidly gaining in acceptance and has already been applied to the

Received 9 March 2013, Accepted 25 March 2013, Scheduled 27 March 2013

* Corresponding author: Krzysztof A. Michalski (krys@ece.tamu.edu).

solution of various challenging engineering tasks, including the EM imaging of buried inhomogeneities [15, 16]. In [15], DE was shown to outperform the state-of-the-art GAs in the imaging of circular-cylindrical conductors and tunnels.

The EM imaging is an iterative procedure, in which the scattered field from a trial object is compared with that of the target. The computation of the field scattered by a known object is referred to as the forward problem. For homogeneous objects, a boundary integral equation (BIE) formulation is often the method of choice. A standard BIE approach requires the solution of a coupled set of integral equations for the equivalent electric and magnetic currents on the surface of the object [17, 18]. These equations are then discretized and solved by a boundary-element method (BEM) [19]. It is also possible to formulate a single integral equation in terms of only one kind of current, and thus reduce the number of unknowns by half [20–25]. In the present paper, we combine the DE algorithm with the single boundary integral equation method (SBIEM) and apply this DE-SBIEM to the problem of EM imaging of buried dielectric cylinders of elliptic cross-section.

The problem under study is defined in Section 2. The single integral equation (SIE) used to solve the forward problem is derived in Section 3, with the details of the BEM procedure relegated to Appendix A. The cost function used in the inverse problem and the DE inversion algorithm are described in Section 4, with the details of the DE included in Appendix B. In Section 5, numerical results are presented, which illustrate the application of the DE-SBIEM to the EM imaging of two sample targets. Conclusions are presented in Section 6.

2. PROBLEM STATEMENT

The geometry of the problem is illustrated in Fig. 1. The cross-section of the dielectric cylinder is assumed to be elliptic, with an arbitrary tilt angle. Attention is limited to the two-dimensional (2-D) case independent of the z coordinate. The bullets in Fig. 1 represent transmitter/receiver line sources, which are arranged in a cross-borehole configuration [26–29]. The study is devoted to deep inclusions, where the effect of the air-ground interface is unimportant. The sources, which are time-harmonic (the $e^{j\omega t}$ time convention is used), may be electric or magnetic, producing an incident field that is, respectively, transverse-magnetic (TM) or transverse-electric (TE) to the cylinder axis. We assume that medium i is characterized by the permeability $\mu_i = \mu_0$ and complex permittivity $\epsilon_i = \epsilon_0\kappa_i - j\sigma_i/\omega$, where ($\mu_0$, ϵ_0) are the free-space parameters and κ_i and σ_i denote the

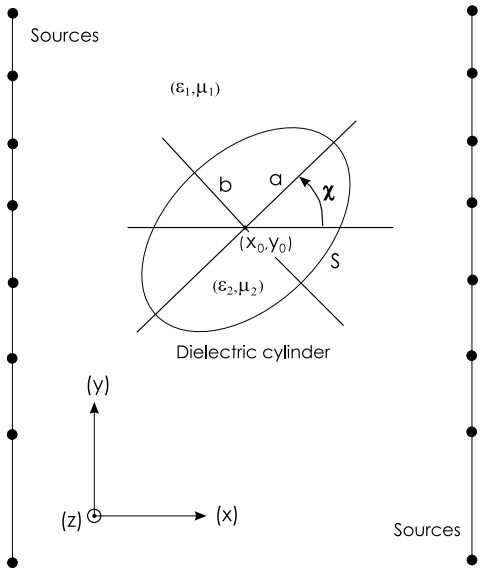

Figure 1. Cross-section view of the target cylinder and the line sources.

dielectric constant and conductivity, respectively. With κ_1 and σ_1 specified, there are seven parameters to be recovered: the dielectric constant κ_2 and conductivity σ_2 of the cylinder, the axis coordinates x_0 and y_0, the major semi-axis a, the minor semi-axis b (or the aspect ratio $e = b/a$), and the tilt angle χ.

3. FORWARD PROBLEM

Although a series solution is in principle possible for elliptic cylinders [30], we have opted for a BIE formulation, because it can easily be extended to arbitrarily shaped cylinders or cylinders in the presence of an interface. To derive the SIE for the problem of Fig. 1 we apply the equivalence principle [31, 17], as illustrated in Fig. 2. The original problem is shown in Fig. 2(a), where the surface S of the object may be arbitrarily shaped and $\hat{\mathbf{n}}$ is the unit normal vector pointing outward from S. The object is excited by known electric and magnetic currents, $\mathbf{J}^{inc}$ and $\mathbf{M}^{inc}$, which, when immersed in an infinite homogeneous medium with parameters (ϵ_1, μ_1), radiate the "incident field" ($\mathbf{E}_1^{inc}$, $\mathbf{H}_1^{inc}$). The total field outside of the obstacle is the sum of the incident field and the "scattered field" ($\mathbf{E}_1^{s}$, $\mathbf{H}_1^{s}$). The total field inside the object is denoted by ($\mathbf{E}_2$, $\mathbf{H}_2$).

In the external equivalent problem of Fig. 2(b), the equivalent currents ($\mathbf{J}_1$, $\mathbf{M}_1$) reside on the surface S embedded in a homogeneous

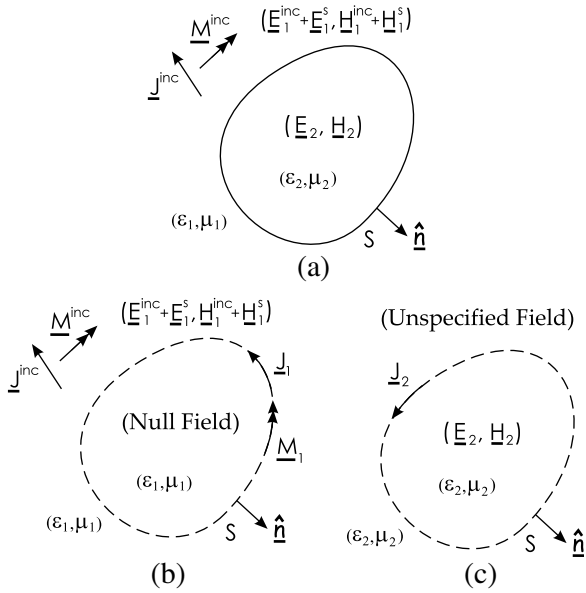

Figure 2. Illustration of the equivalence principle. (a) Original problem. (b) External equivalent problem. (c) Internal equivalent problem.

medium with the parameters (ϵ_1, μ_1). These currents radiate a field ($\mathbf{E}_1$, $\mathbf{H}_1$), which is identical to the scattered field exterior to S, and which cancels the incident field inside S. From the latter condition we obtain

$$\hat{\mathbf{n}} \times \mathbf{E}_1^-[\mathbf{J}_1, \mathbf{M}_1] = -\hat{\mathbf{n}} \times \mathbf{E}_1^{inc} \quad \text{on } S, \tag{1}$$

where the superscript '$-$' indicates that the field is evaluated on the interior side of S. We refer to (1) as the electric field integral equation (EFIE), because $\mathbf{E}_1[\cdot, \cdot]$ is an integral operator. This equation also holds with the electric fields replaced by magnetic fields, in which case it becomes the magnetic field integral equation (MFIE).

In the internal equivalent problem of Fig. 2(c), the *effective* current $\mathbf{J}_2$ resides on the surface S embedded in a homogeneous medium with the parameters (ϵ_2, μ_2). This current radiates the correct field ($\mathbf{E}_2$, $\mathbf{H}_2$) inside S and an unspecified field exterior to S. In view of the continuity of the tangential field components across S, the equivalent currents of the exterior and interior problems are related as [17]

$$\mathbf{J}_1 = \hat{\mathbf{n}} \times \mathbf{H}_2^-[\mathbf{J}_2, 0] \quad \text{on } S, \tag{2}$$

$$\mathbf{M}_1 = \mathbf{E}_2^-[\mathbf{J}_2, 0] \times \hat{\mathbf{n}} \quad \text{on } S. \tag{3}$$

Hence, (1)–(3) constitute an integral equation with a single unknown, $\mathbf{J}_2$.

We now specialize the above to the 2-D case. For the TM excitation, $\mathbf{J}_i = \hat{\mathbf{z}} J_{zi}$, $i = 1, 2$, and $\mathbf{M}_1 = \hat{\boldsymbol{\ell}} M_{\ell 1}$, where $\hat{\mathbf{z}}$ is the unit vector along the cylinder axis and $\hat{\boldsymbol{\ell}}$ denotes the unit vector tangential to the boundary contour C of the cylinder, assumed to be oriented counterclockwise. Also, the electric field is axial and the magnetic field is transverse to z. As a result, we obtain the 2-D counterparts of (1)–(3) as [18, 31]

$$-jk_1\eta_1\langle G_1 J_{z1}\rangle + \left\langle \frac{\partial G_1}{\partial n'} M_{\ell 1} \right\rangle - \frac{M_{\ell 1}}{2} = -E_{z1}^{inc} \quad \text{on } C, \tag{4}$$

$$J_{z1} = -\left\langle \frac{\partial G_2}{\partial n} J_{z2} \right\rangle - \frac{J_{z2}}{2} \quad \text{on } C, \tag{5}$$

$$M_{\ell 1} = -jk_2\eta_2 \langle G_2 J_{z2}\rangle \quad \text{on } C, \tag{6}$$

where the brackets $\langle\rangle$ are used to denote integrals in the source coordinate along the contour C, k_i and η_i are the wavenumber and intrinsic impedance of medium i, and the kernels are defined as

$$G_i = \frac{1}{4j} H_0^{(2)}(k_i R), \tag{7}$$

$$\frac{\partial G_i}{\partial n'} = \frac{k_i}{4j} H_1^{(2)}(k_i R)\, \hat{\mathbf{n}}' \cdot \hat{\mathbf{u}}, \tag{8}$$

$$-\frac{\partial G_i}{\partial n} = \frac{k_i}{4j} H_1^{(2)}(k_i R)\, \hat{\mathbf{n}} \cdot \hat{\mathbf{u}}. \tag{9}$$

Here, $H_n^{(2)}$ is the Hankel function of the second kind and order n. $R = |\mathbf{R}| = |\mathbf{r} - \mathbf{r}'|$, $\mathbf{r}$ and $\mathbf{r}'$ are the position vectors of the field and source points, respectively, and $\hat{\mathbf{u}} = \mathbf{R}/R$. The $1/2 M_{\ell 1}$ and $1/2 J_{z2}$ terms in (4) and (5) are extracted from the singular integrals in the limit as the field point approaches the boundary contour from the inside of the cylinder [18]. The incident field in (4) is found as [31]

$$E_{z1}^{inc} = -\frac{k_1\eta_1}{4} H_0^{(2)}(k_1 R), \tag{10}$$

where we assume a unit-strength line current at $\mathbf{r}'$.

Upon substituting (5) and (6) into (4), we obtain an integral equation with a single unknown, J_{z2}. Once J_{z2} is determined, J_{z1} and $M_{\ell 1}$ follow from (5) and (6), respectively, and the scattered field exterior to the cylinder may be found as

$$E_{z1}^{s} = -jk_1\eta_1\langle G_1 J_{z1}\rangle + \left\langle \frac{\partial G_1}{\partial n'} M_{\ell 1} \right\rangle. \tag{11}$$

The SIE (4)–(6) is transformed by a BEM into a linear algebraic system, which is then solved using a classical LU decomposition. For completeness, the details of the BEM are included in Appendix A.

In TE case, where the cylinder in Fig. 1 is excited by magnetic line currents, we use an SIE based on the MFIE and a magnetic effective current. This TE SIE is dual to the TM SIE developed above, and it may be obtained from the latter by the following replacement of symbols: $E \to H$, $J \to M$, $M \to -J$, and $\eta \to 1/\eta$. We omit the details in the interest of brevity.

Finally, we point out that both SIEs break down at the resonant frequencies of a cavity formed by a perfect conductor covering the surface S and filled with the exterior medium [25, 32]. Although it is possible to derive an SIE free of these irregular frequencies [22], this was unnecessary in the present case, as we limit attention to lossy media, which do not admit real-frequency resonances.

4. INVERSE PROBLEM

Consider the situation as in Fig. 1, where each of the sources can act as a transmitter or a receiver. Our task is to determine the cylinder parameters from the measured fields. Hence, let $\tilde{f}_{ij}$ denote the measured scattered field at receiver j due to transmitter i, where f stands for E^s_{z1} (TM case) or H^s_{z1} (TE case). Similarly, let f_{ij} denote the predicted scattered field for some particular value of the cylinder parameter vector $\mathbf{x} = (\kappa_2, \sigma_2, x_0, y_0, a, e, \chi)$. Then, the solution to the inverse problem may be found by minimizing the cost (or objective) function

$$F(\mathbf{x}) = \sqrt{\frac{\sum_{i=1}^{NS} \sum_{j=i}^{NS} \left| \tilde{f}_{ij} - f_{ij}(\mathbf{x}) \right|^2}{\sum_{i=1}^{NS} \sum_{j=i}^{NS} \left| \tilde{f}_{ij} \right|^2}}. \tag{12}$$

This function is multimodal, i.e., it possesses local minima in addition to the global one, which poses a difficulty for many optimization methods, as they may stagnate within a suboptimal valley. Therefore, this problem is a good candidate for the DE algorithm [11, 13, 33], which is an inherently parallel stochastic search technique.

Just as GAs [4, 5], DE operates on a population of NPOP candidate solutions, or chromosomes. Each chromosome consists of NPAR parameters, or genes, represented by floating-point numbers. (Note that NPAR = 7 in the present case.) Associated with each chromosme is its cost given by (12). The initial population is created in a random fashion and it evolves through a number of generations by mutation, crossover, and selection, with the mutation and crossover controlled by user-specified coefficients C_F and C_R, respectively. The evolution is terminated when either the best population cost falls below the desired tolerance level TOL, or the generation count reaches the

maximum allowed number MAXGEN. The best member of the final population is then hopefully close to the global minimum.

For easy reference, the details of the DE algorithm used in this work are included in Appendix B.

5. NUMERICAL RESULTS

We present sample results for the cross-borehole configuration of Fig. 1, with the two wells located at $x = \pm 2.5$, each comprising an array of 13 sources (hence $NS = 26$) with a separation of 0.5 and with the first source at the $y = 0$ level. (Here and henceforth, all linear dimensions are given in meters.) The sources are either electric (TM case) or magnetic (TE case) with the angular frequency $\omega = 2\pi \times 30 \times 10^6$ [rad/s]. The parameters of the host medium are $\kappa_1 = 12.0$, $\sigma_1 = 10^{-3}$ [S/m]. We consider two target cylinders of elliptic cross-section: a water-filled tunnel (Target 1) and an air-filled tunnel (Target 2). The target parameters and their lower and upper bounds are listed in Tables 1 and 2, respectively.

It is desirable to gauge the accuracy of the forward solution before it used in the inversion procedure. Hence, we have first applied the SBIEM to a circular dielectric cylinder, for which an analytical series solution is available [31]. The cylinder parameters are as given in Table 1, except that $e = 1$ and $\chi = 0°$. We have taken as a measure of the error the objective function (12), in which the reference fields $\tilde{f}_{ij}$ are computed using the exact solution [15], and f_{ij} are obtained by applying the BEM with an increasing number of segments N. These computations were also repeated using the one-point rule in

Table 1. Cylinder parameters and inversion results for Target 1 (water-filled tunnel).

Parameter	κ_2	σ_2	x_0	y_0	a	e	χ
Lower bound	1.0	0.0	−2.0	−5.0	0.05	0.2	0.0°
Upper bound	99.0	1.0	2.0	−1.0	1.05	1.0	180.0°
Target cylinder	80.000	0.100	−0.500	−2.500	0.750	0.670	33.00°
Recovered (TM)	79.639	0.100	−0.501	−2.501	0.750	0.672	33.17°
Recovered (TE)	79.800	0.100	−0.500	−2.500	0.750	0.669	33.03°

Table 2. Cylinder parameters and inversion results for Target 2 (empty tunnel).

Parameter	κ_2	σ_2	x_0	y_0	a	e	χ
Lower bound	1.0	0.0	-2.0	-5.0	0.05	0.2	0.0°
Upper bound	10.0	0.1	2.0	-1.0	1.05	1.0	180.0°
Target cylinder	1.000	0.000	0.000	-2.500	0.750	0.500	120.00°
Recovered (TM)	1.094	0.000	0.000	-2.500	0.752	0.502	119.76°
Recovered (TE)	1.097	0.000	-0.001	-2.500	0.761	0.498	119.17°

the evaluation of the BEM integrals. The resulting convergence plots are shown in Fig. 3. As expected, the accuracy suffers with the one-point approximation in effect. For the same circular cylinder, excited by a unit-strength electric line current located at $(x, y) = (-2.5, 0.0)$, the exact equivalent surface currents are compared in Fig. 4 with those obtained using the SBIEM with $N = 40$. The currents are plotted vs. the arc-length coordinate ℓ (normalized to the free-space wavelength λ_0) along C, which is measured counterclockwise from the point $\chi = 0°$.

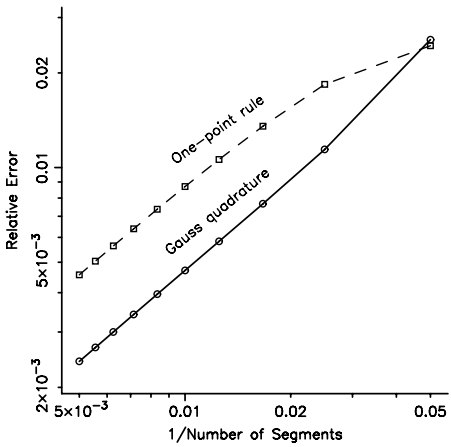

Figure 3. Convergence plots of the SBIEM-computed scattered fields for a circular water-filled cylinder showing the effect of the one-point rule approximation in the computation of the BEM integrals.

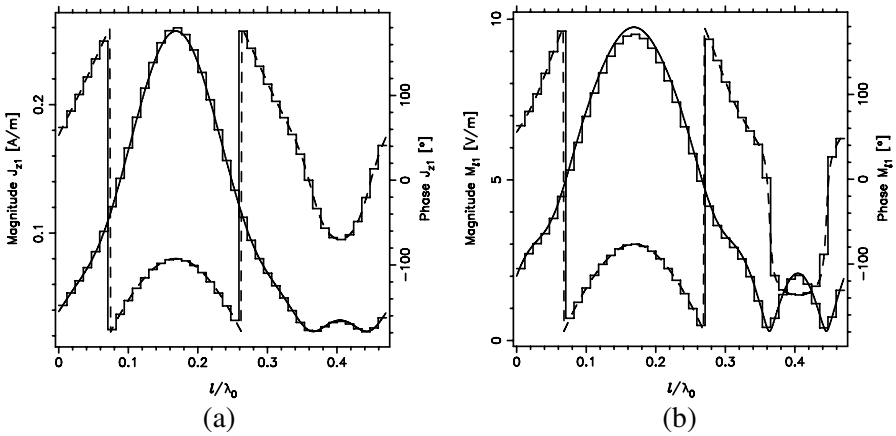

Figure 4. Exact equivalent currents (solid and dashed lines represent magnitude and phase, respectively) for a circular water-filled cylinder are compared with those computed using the SBIEM (staircase lines). (a) J_{z1}. (b) $M_{\ell 1}$.

In the examples that follow, we have used $N = 40$ as a compromise between accuracy and efficiency.

We next turn attention to the inversion procedure. Since the computation of the cost function involves a numerical solution of an integral equation, it is a time consuming process, even with the SBIEM. Hence, we have opted to use a small population size of NPOP $= 5 \times$ NPAR $= 35$. In all cases presented here, we have used the mutation and crossover coefficients $C_F = 0.7$ and $C_R = 0.9$, respectively. These values were arrived at as a result of a limited number of trial runs, and are not necessarily optimal. The termination parameters are TOL $= 2.5 \times 10^{-3}$ and MAXGEN $= 50$. The reference (or "measured") data were generated from (A8), using the parameters of the target cylinder.

The performance of this inversion algorithm for Target 1 under TM illumination is illustrated in Fig. 5, where the target cylinder is shown as a shaded ellipse and the line sources are indicated by bullets. The initial and final cylinder populations are shown if Figs. 5(a) and 5(b), respectively. Observe that the final population is on top of the target.

The DE convergence plots for Targets 1 and 2 under both the TM and the TE illumination are shown in Fig. 6, and the inversion results are included in the last two rows of Tables 1 and 2, respectively. The number of cost function evaluations for the TM/TE cases was 1593/1736 for Target 1, and 1675/1805 for Target 2. In computing these results, we have found that with the one-point approximation

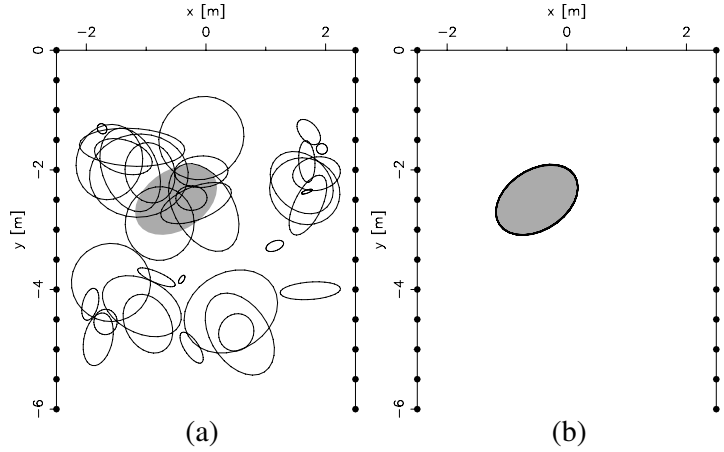

Figure 5. Illustration of the inversion procedure for Target 1 (waterfilled tunnel) under TM illumination. (a) Initial population of cylinders superposed on the shaded target. (b) Final cylinder population superposed on the target.

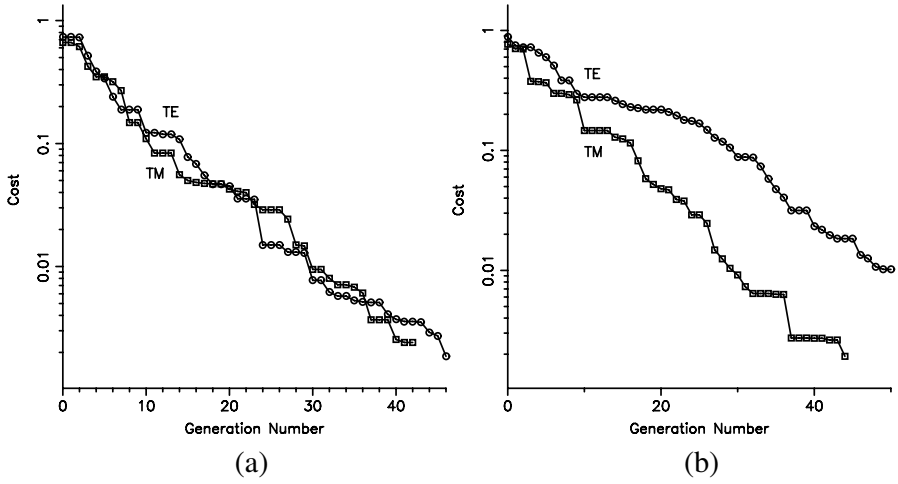

Figure 6. DE convergence plots. (a) Target 1 (water-filled tunnel). (b) Target 2 (empty tunnel).

of the BEM integrals the numerical model is not accurate enough to reflect the small changes in the chromosome values at the later stage of the inversion, causing the DE to stagnate. The DE convergence plots often exhibit a characteristic staircase behavior, with intervals where the cost does not decrease from generation to generation. To mitigate this drawback somewhat, we have implemented an ad hoc hybrid

method, which combines DE with an occasional deterministic descent along the negative gradient of the cost function, with the gradients computed by the finite-difference method [34, 35]. The descent is triggered with a probability of 0.5 each time the best cost does not decrease between consecutive generations. This accelerated DE was used to obtain the results presented here.

From the two targets considered, Target 2 (the air-tunnel) proved to be more challenging, presumably because it presents a much weaker contrast to the incident field than Target 1. With the same parameter bounds as those used for Target 1 (see Table 1) and the small population size used, DE tends to get trapped in a local minimum corresponding to a small-radius lossy cylinder, which apparently produces a scattered field very similar to that of the target. Under the TM illumination, the inversion of the air-tunnel was successful with a narrower search space for the dielectric constant and conductivity, as indicated in Table 2. In the TE case, however, the inversion failed to converge within MAXGEN = 50 generations, as can be seen in Fig. 6(b). This slow convergence may be explained by the fact that the air cylinder of electrically small cross-section is weakly excited by a TE polarized field. Hence, the numerical model employed in the forward problem may be too crude in this case to accurately reflect the minute parameter adjustments required as the inversion procedure homes on the target.

In summary, our preliminary results have shown that the DE-SBIEM-based imaging can be remarkably accurate and efficient. Moreover, for a method which does not require a good "first-guess" solution, the procedure is reasonably robust.

6. CONCLUSION

We have demonstrated simultaneous electromagnetic (EM) inversion of the location, shape, and complex dielectric constant of two-dimensional dielectric cylinders of elliptic cross-section using the differential evolution (DE) algorithm combined with the single boundary integral equation method (SBIEM). Simulation results have been presented which demonstrate that the DE-SBIEM offers a conceptually simple yet efficient and reasonably robust technique for the imaging of buried objects and voids. The method requires a certain amount of problem-dependent tuning, mainly to adjust the mutation and crossover coefficients. Premature convergence or stagnation can occur with the small population sizes likely to be employed if the cost function is computationally expensive. This may require ad hoc devices, such as deterministic descents and re-starts with refreshed populations, to

improve the efficiency and reliability of the method. These drawbacks notwithstanding, this study indicates that DE-SBIEM offers much promise for EM imaging applications. Future research should explore the feasibility of this method for the imaging of arbitrarily shaped objects.

APPENDIX A. BOUNDARY-ELEMENT METHOD

In the BEM, the cylinder contour C is approximated by N straight segments, as illustrated in Fig. A1, and the surface currents are expanded as

$$J_{zi} = \sum_{n=1}^{N} I_n^i P_n, \quad M_{\ell 1} = \sum_{n=1}^{N} K_n^1 P_n, \tag{A1}$$

where $i = 1, 2$, and P_n is a unit pulse over segment n [19, 36, 37]. Upon substituting (A1) into (4)–(6) and point-matching the resulting equations at segment center points, we obtain an $N \times N$ algebraic system

$$\Big[\big[Z^{EJ1}\big]\big[Z^{HJ2}\big] + \big[Z^{EM1}\big]\big[Z^{EJ2}\big]\Big]\big[I^2\big] = -\big[V^1\big], \tag{A2}$$

with the matrix elements given as

$$Z_{mn}^{EJi} = -\frac{k_i \eta_i}{4}\Big\langle H_0^{(2)}(k_i R_m)\Big\rangle_n, \quad i = 1, 2, \tag{A3}$$

$$\begin{aligned} Z_{mn}^{EM1} &= \frac{k_1}{4j}\Big\langle H_1^{(2)}(k_1 R_m)\sin(\Omega_n - \Psi_m)\Big\rangle_n, \quad m \neq n, \\ &= -\frac{1}{2}, \quad m = n, \end{aligned} \tag{A4}$$

$$\begin{aligned} Z_{mn}^{HJ2} &= \frac{k_2}{4j}\Big\langle H_1^{(2)}(k_2 R_m)\sin(\Omega_m - \Psi_m)\Big\rangle_n, \quad m \neq n, \\ &= -\frac{1}{2}, \quad m = n. \end{aligned} \tag{A5}$$

Here, $\langle\,\rangle_n$ indicates integration over the nth segment of C, $R_m = |\mathbf{R}_m|$, where $\mathbf{R}_m$ is the vector from the source point on segment n to the center point of segment m, and Ω_n and Ψ_m are the inclination angles of segment n and $\mathbf{R}_m$, respectively, as illustrated in Fig. A1. The elements of the excitation vector in (A2) are given as

$$V_m^1 = -\frac{k_1 \eta_1}{4} H_0^{(2)}(k_1 R_m), \tag{A6}$$

where $\mathbf{R}_m$ is the vector from the line source to the match point on segment m.

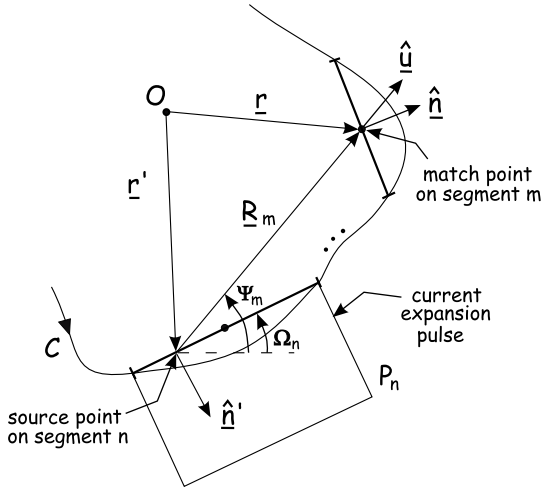

Figure A1. Straight-segment model of the boundary contour C of a cylinder and the associated quantities.

Once (A2) is solved for $\left[I^2\right]$, the current expansion coefficients of the external equivalent problem are obtained as

$$\left[I^1\right] = \left[Z^{HJ2}\right]\left[I^2\right], \quad \left[K^1\right] = \left[Z^{EJ2}\right]\left[I^2\right]. \tag{A7}$$

Finally, the scattered field at the NS receiver locations is obtained from

$$\left[E^s_{z1}\right] = \left[Z^{EJ1}\right]\left[I^1\right] + \left[Z^{EM1}\right]\left[K^1\right], \tag{A8}$$

which is a discretized version of (11). In the above, the matrix elements Z^{EJ1}_{mn} and Z^{EM1}_{mn} are given by (A3) and (A4), respectively, with the understanding that m refers to the mth receiver location, and that the first expression in (A4) is used for *all* indices m and n.

The integrals in (A3)–(A5) are computed by low-order Gauss-Legendre quadratures, except for the case $m = n$ in (A3), when the integral is evaluated by a quadrature especially developed for logarithmically singular integrands [38]. In a more efficient but less accurate approach, the singular integrals are evaluated analytically using a small-argument form of the Hankel function, and the remaining integrals are approximated using a one-point rule [19].

APPENDIX B. DIFFERENTIAL EVOLUTION

DE operates on a population of candidate solutions by applying mutation, crossover (or recombination), and selection. Each individual (or chromosome) $\mathbf{x}^P_i$, $i = 1, 2, \ldots,$ NPOP, of population P is a vector $(x^P_{i,1}, x^P_{i,2}, \ldots, x^P_{i,\mathrm{NPAR}})$ of NPAR parameters (or genes) represented by

floating-point numbers. The size of the population, NPOP, is selected by the user, with typical values between $2\times$ and $100\times$NPAR. The DE algorithm [11, 13, 33] consists of the following steps:

(i) The initial population is generated according to

$$x_{i,j}^P = x_j^{\text{MIN}} + R_j \left(x_j^{\text{MAX}} - x_j^{\text{MIN}}\right), \quad j = 1, 2, \ldots, \text{NPAR}, \quad \text{(B1)}$$

where $R_j \in [0, 1]$ is a random number with a uniform distribution, where x_j^{MIN} and x_j^{MAX} denote the minimum and maximum permissible values of the jth parameter, respectively. The costs $F\left(\mathbf{x}_i^P\right)$ of all individuals is evaluated.

(ii) For each target individual (or *primary parent*) $\mathbf{x}_i^P$, a mutant vector $\mathbf{v}_i^P$ is formed according to

$$\mathbf{v}_i^P = \mathbf{x}_{i_B}^P + C_F\left(\mathbf{x}_{r_2}^P - \mathbf{x}_{r_1}^P\right), \quad \text{(B2)}$$

where i_B is the index of the best individual (the one with the lowest cost). r_1 and r_2 are randomly selected distinct indices from the range [1, NPOP] and different from i, and C_F is a user-supplied mutation factor with the suggested range [0.4, 1]. In this operation, a *secondary parent* $\mathbf{x}_{i_B}^P$ is perturbed by a randomly selected differential.

(iii) A trial vector (or *child*) $\mathbf{u}_i^P$ is formed with the jth parameter generated as follows:

$$u_{i,j}^P = \begin{cases} v_{i,j}^P & \text{if } R_j \le C_R, \\ x_{i,j}^P & \text{otherwise,} \end{cases} \quad \text{(B3)}$$

where $R_j \in [0, 1]$ is a uniform random number and $C_R \in [0, 1]$ a user-specified recombination constant, which is typically close to 1. The *binary* crossover (B3) is monitored to detect if $\mathbf{u}_i^P$ gets at least one gene from the mutant vector $\mathbf{v}_i^P$. Should this not be the case, a random index $j \in [1, \text{NPAR}]$ is generated and $u_{i,j}^P$ is set to $v_{i,j}^P$. If the newly generated parameter $u_{i,j}^P$ falls outside the range $[x_j^{\text{MIN}}, x_j^{\text{MAX}}]$, it is replaced by a feasible value, which may be a half-way point between the violated bound and the previous gene value. Finally, the cost $F(\mathbf{u}_i^P)$ is evaluated.

(iv) The child competes with the parent for the right to propagate to the next generation:

$$\mathbf{x}_i^{P+1} = \begin{cases} \mathbf{u}_i^P & \text{if } F\left(\mathbf{u}_i^P\right) < F\left(\mathbf{x}_i^P\right), \\ \mathbf{x}_i^P & \text{otherwise.} \end{cases} \quad \text{(B4)}$$

(v) The steps 2–4 are repeated until the best population cost falls below the desired tolerance level TOL or the generation count reaches the specified maximum number MAXGEN.

The algorithm just summarized is designated DE/best/1/bin [13], because the best individual is used for the secondary parent, one differential is involved in the mutation, and the crossover is binary. There are other variants of DE, which use different strategies to form the mutant vectors and different ways to perform the crossover (which could be exponential, rather than binary) [11]. For example, in DE/rand/1/bin, the secondary parent is selected randomly from the current population.

It is perhaps worthwhile to point out some differences between the DE and traditional, real-coded genetic algorithms (GAs) [33, 34, 39]. First, DE does not involve selection of parents based on fitness. The primary parent is chosen deterministically: each individual of the current generation becomes a primary parent exactly once. A crossover with a mutated secondary parent creates one child, not two, as in most GAs. This child is only compared to one individual: its primary parent, not to all the individuals in the current population, and the fitter one wins a spot in the next generation. As a result, all the individuals of the next generation are as good or better than their counterparts in the current generation, which obviates the elitist strategy widely used in GAs.

The most important difference, however, is in the nature of the mutation, which in DE is the first step, while in GAs it is the last. In GAs, mutation takes the form of a random perturbation of a fixed type; for example, in real-coded GAs, a gene value is augmented by a random fraction of its allowed range. Such a perturbation, whose purpose is to prevent premature convergence, can be needlessly destructive. DE avoids this problem by mutating secondary parents with population-derived difference vectors. As generations pass, these differentials tend to adapt to the natural scaling of the problem. For example, if the population becomes compact in one variable but remains widely dispersed in another, the differentials sampled from it will be small in the first variable yet large in the other. This automatic adaptation significantly improves the convergence of the algorithm.

REFERENCES

1. Kleinman, R. E. and P. M. van den Berg, "Two-dimensional location and shape reconstruction," *Radio Sci.*, Vol. 29, No. 4, 1157–1169, 1994.

2. Franchois, A. and C. Pichot, "Microwave imaging-complex permittivity reconstruction with Levenberg-Marquardt method," *IEEE Trans. on Antennas and Propagat.*, Vol. 45, 203–215, Feb. 1997.
3. Bonnard, S., P. Vincent, and M. Saillard, "Inverse obstacle scattering for homogeneous dielectric cylinders using a boundary finite-element method," *IEEE Trans. on Antennas and Propagat.*, Vol. 48, 393–400, Mar. 2000.
4. Haupt, R. L. and S. E. Haupt, *Practical Genetic Algorithms*, Wiley, New York, 1998.
5. Rahmat-Samii, Y. and E. Michielssen, *Electromagnetic Optimization by Genetic Algorithms*, Wiley, New York, 1999.
6. Chiu, C. and P. Liu, "Electromagnetic transverse electric-wave inverse scattering of a conductor by a genetic algorithm," *Int. J. Imag. Syst. Techn.*, Vol. 9, No. 5, 388–394, 1998.
7. Qing, A. and C. K. Lee, "Microwave imaging of a perfectly conducting cylinder using a real-coded genetic algorithm," *IEE Proc. — Microw. Antennas Propagat.*, Vol. 146, 421–425, Dec. 1999.
8. Qing, A., C. K. Lee, and L. Jen, "Microwave imaging of parallel perfectly conducting cylinders using real-coded genetic algorithm," *Journal of Electromagnetic Waves and Applications*, Vol. 13, No. 8, 1121–1143, 1999.
9. Meng, Z. Q., T. Takenaka, and T. Tanaka, "Image reconstruction of two-dimensional impenetrable objects using genetic algorithm," *Journal of Electromagnetic Waves and Applications*, Vol. 13, No. 1, 95–118, 1999.
10. Caorsi, S. and M. Pastorino, "Two-dimensional microwave imaging approach based on a genetic algorithm," *IEEE Trans. on Antennas and Propagat.*, Vol. 48, 370–373, Mar. 2000.
11. Price, K. V., "An introduction to differential evolution," *New Ideas in Optimization*, D. Corne, M. Dorigo, and F. Glover, Eds., Ch. 6, 79–108, McGraw-Hill, 1999.
12. Qing, A., *Differential Evolution, Fundamentals and Applications in Electrical Engineering*, Wiley, Singapore, 2009.
13. Storn, R. and K. Price, "Differential evolution — A simple and efficient heuristic for global optimization over continuous spaces," *J. Glob. Opt.*, Vol. 11, 341–359, 1997.
14. Tvrdík, J. and I. Křivý, "Simple evolutionary heuristics for global optimization," *Comput. Stat. Data Anal.*, Vol. 30, 345–352, May 1999.

15. Michalski, K. A., "Electromagnetic imaging of circular-cylindrical conductors and tunnels using a differential evolution algorithm," *Microwave & Opt. Technol. Lett.*, Vol. 26, Dec. 5, 2000.
16. Michalski, K. A., "Electromagnetic imaging of elliptical-cylindrical conductors and tunnels using a differential evolution algorithm," *Microwave & Opt. Technol. Lett.*, Vol. 27, Feb. 5, 2001.
17. Harrington, R. F., "Boundary integral formulations for homogeneous material bodies," *Journal of Electromagnetic Waves and Applications*, Vol. 3, No. 1, 1–15, 1989.
18. Morita, N., N. Kumagai, and J. R. Mautz, *Integral Equation Methods for Electromagnetics*, Artech House, Norwood, MA, 1990.
19. Peterson, A. F., S. L. Ray, and R. Mittra, *Computational Methods for Electromagnetics*, IEEE Press, New York, 1998.
20. Marx, E., "Integral equation for scattering by a dielectric," *IEEE Trans. on Antennas and Propagat.*, Vol. 32, 166–172, Feb. 1984.
21. Glisson, A. W., "An integral equation for electromagnetic scattering from homogeneous dielectric bodies," *IEEE Trans. on Antennas and Propagat.*, Vol. 32, 173–175, Feb. 1984.
22. Mautz, J. R., "A stable integral equation for electromagnetic scattering from homogeneous dielectric bodies," *IEEE Trans. on Antennas and Propagat.*, Vol. 37, 1070–1071, Aug. 1989.
23. Swatek, D. R. and I. R. Ciric, "Single source integral equation for wave scattering by multiply-connected dielectric cylinders," *IEEE Trans. on Magn.*, Vol. 32, 878–881, May 1996.
24. Pelosi, G. and G. Toso, "A boundary element approach to the scattering from inhomogeneous dielectric bodies," *IEEE Trans. on Antennas and Propagat.*, Vol. 46, 602–603, Apr. 1998.
25. Yeung, M. S., "Single integral equation for electromagnetic scattering by three-dimensional homogeneous dielectric objects," *IEEE Trans. on Antennas and Propagat.*, Vol. 47, 1615–1622, Oct. 1999.
26. Newman, G., "Crosswell electromagnetic inversion using integral and differential equations," *Geophys.*, Vol. 60, No. 3, 899–911, 1995.
27. Ellis, G. A. and I. C. Peden, "Cross-borehole sensing: Identification and localization of underground tunnels in the presence of a horizontal stratification," *IEEE Trans. on Geosci. Remote Sensing*, Vol. 35, 756–761, May 1997.
28. Bonnard, S., P. Vincent, and M. Saillard, "Cross-borehole inverse scattering using a boundary finite-element method," *Inverse Problems*, Vol. 14, No. 3, 521–534, 1998.

29. Choi, H. and J. Ra, "Detection and identification of a tunnel by iterative inversion from cross-borehole CW measurements," *Microwave & Opt. Technol. Lett.*, Vol. 21, No. 6, 458–465, 1999.
30. Caorsi, S., M. Pastorino, and M. Raffetto, "EM field prediction inside lossy multilayer elliptic cylinders for biological-body modeling and numerical-procedure testing," *IEEE Trans. on Biomed. Eng.*, Vol. 46, 1304–1309, Nov. 1999.
31. Harrington, R. F., *Time-harmonic Electromagnetic Field*, McGraw-Hill, New York, 1961.
32. Arvas, E. and J. R. Mautz, "On the non-uniqueness of the surface EFIE applied to multiple conducting and/or dielectric bodies," *Arch. Elek. Übertragung.*, Vol. 42, No. 6, 364–369, 1988.
33. Price, K. and R. Storn, "Differential evolution," *Dr. Dobb's J.*, 18–24, Apr. 1997.
34. Masters, T. and W. Land, "A new training algorithm for the general regression neural network," *1997 IEEE International Conference on Systems, Man, and Cybernetics, Computational Cybernetics and Simulation*, 1990–1994, Oct. 1997.
35. Chiou, J. and F. Wang, "Hybrid method of evolutionary algorithm for static and dynamic optimization problems with application to a fed-batch fermentation process," *Comp. Chem. Engng.*, Vol. 23, 1277–1291, 1999.
36. Arvas, E., S. M. Rao, and T. K. Sarkar, "*E*-field solution of TM-scattering from multiple perfectly conducting and lossy dielectric cylinders of arbitrary cross-section," *IEE Proceedings, Part H — Microwaves, Antennas and Propagation* , Vol. 133, 115–121, Apr. 1986.
37. Arvas, E., Y. Qian, A. Sadigh, T. K. Sarkar, and F. Aslan, "E-field and H-field solutions of TE scattering from multiple conducting and dielectric cylinders of arbitrary cross-section," *Journal of Electromagnetic Waves and Applications*, Vol. 3, No. 6, 513–530, 1989.
38. Crow, J. A., "Quadrature of integrands with a logarithmic singularity," *Math. Comp.*, Vol. 60, 297–301, Jan. 1993.
39. Chang, C. S. and D. Du, "Further improvement of optimisation method for mass transit signalling block-layout design using differential evolution," *IEE Proc. — Electr. Power Appl.*, Vol. 146, 559–569, Sept. 1999.